colloids and interfaces

MDPI

Article

H_2O/D_2O Contrast Variation for Ultra-Small-Angle Neutron Scattering to Minimize Multiple Scattering Effects of Colloidal Particle Suspensions

Akira Otsuki [1,*], Liliana de Campo [2], Christopher J. Garvey [2] and Christine Rehm [2,3]

[1] Ecole Nationale Supérieure de Géologie, GeoRessources UMR 7359 CNRS, University of Lorraine, 2 Rue du Doyen Marcel Roubault, BP 10162, 54505 Vandoeuvre-lès-Nancy, France
[2] Australian Centre for Neutron Scattering, Australian Nuclear Science and Technology Organisation, Lucas Heights, New South Wales 2234, Australia; liliana.decampo@ansto.gov.au (L.d.C.); cjg@ansto.gov.au (C.J.G.); christine.rehm@gtiit.edu.cn (C.R.)
[3] Guangdong Technion Israel Institute of Technology, 241 Da Xue Road, Shantou 515063, Guangdong Province, China
* Correspondence: akira.otsuki@univ-lorraine.fr; Tel.: +33-372-744-543

Received: 20 August 2018; Accepted: 5 September 2018; Published: 7 September 2018

Abstract: This study investigated the use of solvent contrast (H_2O/D_2O ratio) as a means to optimize the ultra-small-angle neutron scattering (USANS) signal. By optimizing the signal, it was possible to reduce the undesirable effects of coherent multiple scattering while still maintaining a measurable scattered intensity. This result will further enable the use of USANS as a probe of the interactions between colloidal particles and their structures within concentrated suspensions as well as particle dispersion/aggregation. As a model system, we prepared silica colloidal particle suspensions at different solid concentrations. USANS curves were measured using the classical Bonse–Hart double crystal diffractometer while varying the scattering length density of the aqueous phase, thus varying the contrast to the silica particles. As a means of assessing the impact of multiple scattering effects on different q-values, we analyzed the scattered intensity at different contrasts at three different q values. The data were then used to determine the match point of the silica particle suspensions from the expected square root dependence of the scattered intensity with solvent composition, to analyze any differences associated with the solid concentration change, and to determine the optimum H_2O/D_2O ratio in terms of high transmission (T_{SAS} > 80%) and high enough scattering intensity associated with the contrast of the system. Through this investigation series, we confirmed that adjusting the contrast of the solvent (H_2O/D_2O) is a good methodology to reduce multiple scattering while maintaining a strong enough scattering signal from a concentrated suspension of silica particles for both USANS and rheometric USANS (rheo-USANS) experiments.

Keywords: silica; rheo-SANS; q-dependency; scattering length density; T_{SAS} value; solid concentration

1. Introduction

Concentrated colloidal particle suspensions are found in a wide range of daily products (e.g., milk, cosmetics) and industrial products/processes (e.g., mineral pulp, drug production). Precise understanding and manipulation of interactions within such a particle suspension and its resulting bulk behavior are thus of great interest and importance in both science and engineering. In this work, our primary interest is submicron to micron size particle aqueous suspensions relevant to the current and long-lasting challenges associated with colloidal particle processing/separation (e.g., [1]) and their characterization methods (e.g., [2,3]).

The majority of characterization methods either requires some special sample preparation, or those suitable for direct characterization of particle behavior in a solution require a very small volume fraction

of particles (e.g., 1×10^{-5} vol % for dynamic light scattering [4]) due to the strength of the interaction between light and the particle suspension [5]. Furthermore, when the linkage between microscopic structure and bulk properties of a suspension is affected by an external field, such as a shear field, techniques which can probe structure in situ are highly desirable. A related difficulty is to precisely quantify the interactions in concentrated colloidal particle suspensions commonly prepared/processed in actual plant operations (e.g., [6,7]) from the extrapolation of dilute solution studies.

Small-angle neutron scattering (SANS) methods have the potential to probe bulk average structures in a concentrated colloidal particle suspension/dispersion and allow us to understand and quantify the particle–particle interactions [8]. Scattering curves are interpreted in terms of the angular or q-dependence of the scattered intensity [9].

$$q = \frac{4\pi}{\lambda} \sin\left(\frac{\theta}{2}\right) \tag{1}$$

where θ is the scattering angle and λ is the wavelength of the scattered radiation.

However, at high solid/particle concentrations, multiple scattering may hinder extracting the desired structural information directly from the interpretation of SANS curves due to the consequential q-dependent distortion of the measured scattered intensity [10]. If multiple scattering occurs for a given particle/solvent system, it attenuates scattering of the incident beam that should be going in a given (forward) direction and, therefore, distorts the signal which would have been recorded in the limit of single scattering. It follows that the straightforward relationship between the differential cross section and the pair correlation function, i.e., between the structure of the material and the measured scattering signal, is lost [11]. While a typical approach to reduce multiple scattering is either or both (a) reducing the particle concentration and/or (b) reducing the sample path length, they have obvious limitations in (i) using the behavior of less concentrated suspension to understand the more concentrated suspension; (ii) difficulty in proper feeding of a viscous suspension (in other words, heterogeneity as well as the impact of the sample cell geometry on the structure could affect the sample subjected to the beam and, thus, produce a misleading result); and (iii) the increasing volumetric effect of the surface perturbation of two cell faces on the decreasing bulk of thinner samples. On the other hand, for neutron scattering experiments, it is possible to optimize the scattering strength of a sample by decreasing the contrast between the two phases, particulate, and solvent (water) in a way that is analogous to the role of refractive index adjustment in light scattering [12]. In this study, we adjusted the scattering length density of the solvent by varying the H_2O/D_2O composition, i.e., by contrast variation (e.g., [13]). In other words, we utilized the difference between the neutron scattering length densities (SLD) of H_2O (-0.50×10^{-6} Å^{-2} [14]) and D_2O (6.37×10^{-6} Å^{-2} [14]) in order to adjust the scattering power of the sample, and thus to minimize the effects of multiple scattering. To the best of the authors' knowledge, systematic and extensive study of this approach has been very limited. Apart from optimizing sample preparation, multiple scattering effects may also be corrected for during data processing. For that, a variety of procedures is available such as analytical approximations as discussed by, (e.g., [15–23]). The multiple scattering of neutrons has also been studied using the technique of Monte Carlo simulation (e.g., [24–27]). Additionally, in the case of thick samples, a partial correction for the effect of multiple scattering can be done using an empirical approach (e.g., [28,29]), where various thicknesses of one sample are measured, the data fitted—possibly using the equation described by Vineyard (1954) [15]—and multiple scattering from a sample of known thickness accordingly corrected for.

In this article, we report our investigation on using a H_2O/D_2O contrast variation in conjunction with ultra-small-angle neutron scattering (USANS) to limit the effects of coherent multiple scattering while maintaining strong enough scattering that can be utilized to understand the particle–particle interactions and particle dispersion/aggregation within highly concentrated colloidal suspensions. Multiple incoherent scattering is out of our concern in this study since it contributes only to the background and can be tolerated. Particle interactions and dispersions/aggregations will be separately reported in detail, and thus

are outside the scope of this article. The experiments were performed first in a flat tumbling cell to ensure homogeneous particle dispersion without particle sedimentation. Then, similar measurements were performed in a rheo-USANS sample cell with a Couette geometry [30]. The series of investigations showed that contrast variation was able to continuously vary the scattering power of a sample, allowing for an optimization between minimizing multiple scattering and maximizing the scattering power of the sample. This is particularly useful in the case where the sample thickness is fixed and cannot be adjusted—e.g., for rheo-USANS measurements. In this study, the existence and degree of multiple scattering effects in samples were determined via (a) the linearity of the square root of the scattered intensity as a function of H_2O vol % in H_2O/D_2O ratio, as well as (b) sample transmission, T_{SAS}. The T_{SAS} value will be defined and explained in the results and discussion section.

2. Materials and Methods

USANS experiments were performed on the Kookaburra beamline on the cold-neutron guide CG3 at the Australian Centre for Neutron Scattering, Australian Nuclear Science and Technology Organisation [31,32], with a monochromatic wavelength of 4.74 Å. Kookaburra is based on the Bonse–Hart method [33] and utilizes two identical, multi-bounce, channel-cut, perfect Si single crystals labelled 'monochromator' and 'analyzer' (arranged in non-dispersive or parallel geometry) in Bragg reflection, see Figure 1. When the monochromator and analyzer crystals are aligned (analyzer deviation angle $\theta = 0°$, i.e., the analyzer crystal is in the 'peak position'), an incident neutron beam is totally reflected into the main detector. In addition to the main detector, a transmission detector is in use to monitor the intensity of the neutron beam transmitted through the sample, including all neutrons scattered to low angles apart from the q-value that is reflected onto the main detector.

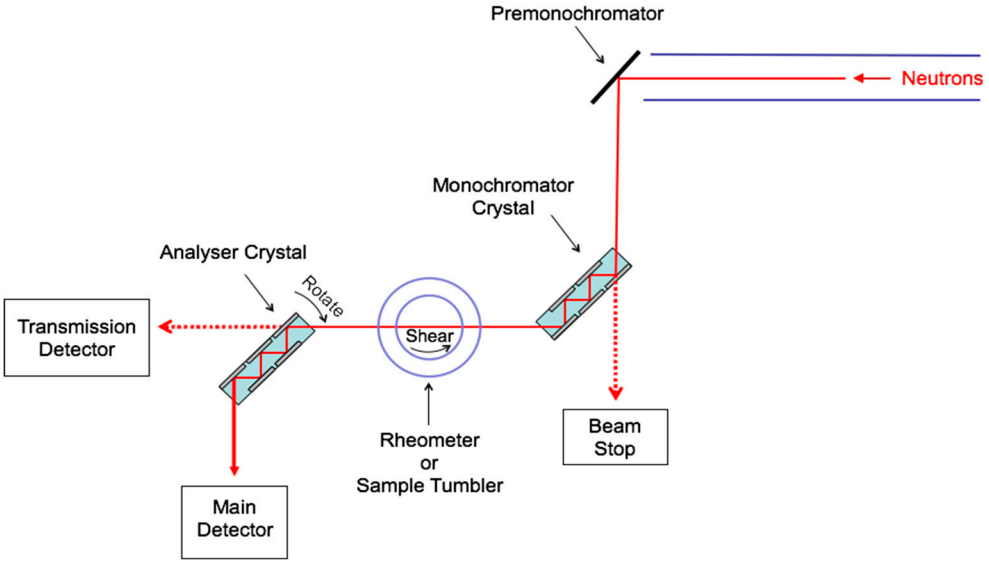

Figure 1. Sketch of the Kookaburra USANS instrument layout.

In a typical USANS experiment rocking curve profiles are measured by rotating the analyzer crystal across the peak position and measuring the neutron intensity as a function of the momentum transfer (or scattering vector) q at which data are collected at one value of q (or θ) at a time. q is related to the rotation or scattering angle θ via Equation (1).

Note that the Bonse–Hart USANS technique as applied on Kookaburra is only sensitive to scattering in one direction, while in the perpendicular direction the measurements are averaged over the possible wavevector transfers, i.e., Kookaburra measures scattered intensity from the sample with excellent angular resolution horizontally of a few arcseconds but with a large acceptance in the vertical direction of a few

degrees, which is described as 'slit smearing'. The high angular resolution required for USANS experiments is enhanced through multiple reflections of the neutron beam before and after the sample.

In this study, two different sample cell setups were used and a series of silica particle suspensions were measured. The first one is an aluminum cell with a neutron path length of 0.5 mm and quartz windows of 4 cm diameter, which was mounted onto a sample tumbler to avoid the effects of sample sedimentation, and the beam was shaped by a Gadolinium aperture of 30 mm diameter. The second one is a Couette quartz flow cell, outer diameter 54 mm, with the Anton-Paar MCR 500 rheometer accepting the neutron beam in the normal (perpendicular) direction (Figure 1). A 25 mm circular Cd aperture was mounted directly in front of the curved Couette cell, and its effective path length was experimentally determined from a comparison of the scattering curves between the Couette and flat cells. The Couette cell has a nominal gap of 0.5 mm, leading to a total beam path of 1 mm theoretically (0.5 mm on each side). However, it should be noted that the effective path length can be slightly longer because the Couette cell is curved, which is particularly important for the large apertures as used here.

Silica particles purchased from Sigma-Aldrich (St. Louis, MO, USA) with a size distribution of 0.5–10 µm—with approximately 80% of particles between 1–5 µm—were used to create sample/aqueous suspensions. Their physical properties are: D_{50} (average particle diameter measured by laser diffraction) is 2.4 µm, BET surface area is 5.2 m^2/g, and density is 2.6 g/cm^3. The literature value of the scattering length density of silica is 4.1×10^{-6} $Å^{-2}$ [14]. USANS measurements were conducted in the q-range from 3.5×10^{-5} to 0.01 $Å^{-1}$. Silica particle suspensions were prepared in an electrolyte solution of potassium nitrate (1×10^{-2} M) consisting of milli-Q water and D_2O in different volume ratios. Solid concentrations were adjusted to between 5 and 40 vol % in order to investigate whether there is any influence on the optimization of the H_2O/D_2O ratio. Once a suspension was evenly mixed, its pH value was adjusted to 10 using 1M and/or 0.1 M KOH in D_2O. The suspension was then mixed by magnetic stirring for 30 min. The suspension was then transferred to a flat cell for USANS measurements or a cylindrical cell (Couette geometry) for rheo-USANS measurements. Experimental rocking curves were reduced and normalized to absolute intensity scale using the standard procedure [34] adapted to Kookaburra using Python scripts on the Gumtree platform [35].

3. Results and Discussion

Figures 2 and 3 show the results of contrast variation with 5 and 10 vol % SiO_2 at pH 10, respectively. Figure 2a shows the absolutely scaled slit-smeared intensity for a H_2O/D_2O contrast variation series to investigate its effect on the scattering intensity and transmission of samples with 5 vol % silica. All the curves are fairly featureless which would be anticipated from the polydisperse silica samples. Starting from a 30/70 H_2O/D_2O mixture, the signal increases with increasing H_2O content, and therefore contrast. It should be noted that the error bars are given in all the figures in this article, but they are mostly smaller than experimental dot points.

The first step of this investigation was to determine q-dependence of the match point, i.e., the contrast, H_2O/D_2O ratio, where the scattered intensity is equal to 0. To extract the potentially q-dependent match point from the data, the intensities at three q-values (1.0×10^{-4}, 2.6×10^{-4}, 6.7×10^{-4} $Å^{-1}$) from each scattering pattern were plotted as a function of H_2O vol % in H_2O/D_2O ratio. As an approximation, the square root of the intensity is expected to give a linear relationship with the H_2O vol % [36,37], as plotted in Figure 2b. For a group of identical, randomly oriented particles, the intensity of coherent, elastic scattering is dependent only on the magnitude of the scattering momentum transfer q, and is defined as [11]

$$I(q) = N\left(\Delta\overline{\mathrm{SLD}}V\right)^2 P(q)S(q) \quad (2)$$

N is the number of particles per unit volume, V is the volume of the particles, $P(q)$ is a form factor that depends on the shape of the particles, $S(q)$ is a structure factor that dictates the inter-particle correlation structure, and $\Delta\overline{\mathrm{SLD}}$ is the scattering density difference between the scattering particles

and solvent. Thus, one can deduce the correlation between the scattering intensity and scattering density difference as

$$I(q) \propto \left(\Delta\overline{\mathrm{SLD}}\right)^2 \tag{3}$$

$$\pm\sqrt{I(q)} \propto \Delta\overline{\mathrm{SLD}} \tag{4}$$

The Equation (4) is used to construct those plots in Figures 2b and 3b.

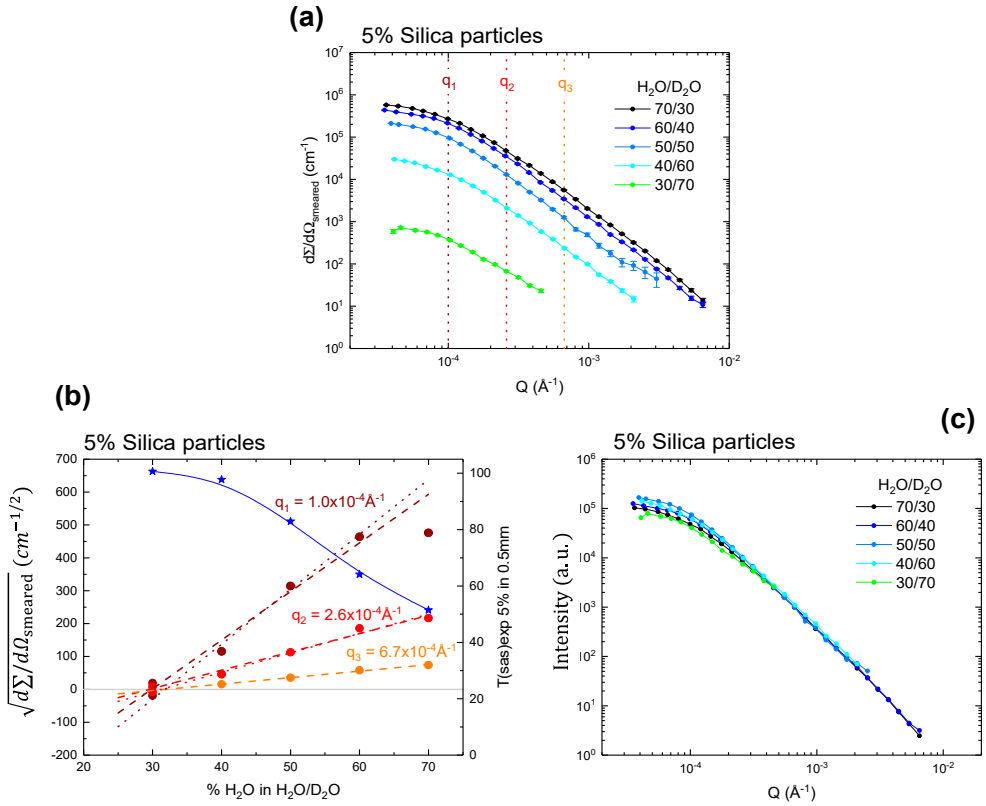

Figure 2. Contrast variation with 5 vol % SiO_2 at pH 10. (**a**) Scattering curves of samples with different H_2O/D_2O ratios; (**b**) left axis: the square root of the scattering intensity as a function of vol % H_2O in H_2O/D_2O ratio and q value (brown, red and orange symbols for the three distinct q-values). The fitted line corresponds to the data with a positive sign (dashed line) and negative sign (dotted line) sign for the first point, respectively. Right axis: $T_{SAS,exp}$ in 0.5 mm path length (blue stars) as a function of vol % H_2O in H_2O/D_2O ratio; (**c**) a plot of the scattering curves from (**a**) normalized to the same value at high q.

The sign of the square root of the intensity for the 30% H_2O sample may be positive or negative, and so both values are plotted. From the linear behavior of all plots, it can be concluded that the match point does not have any q dependency. The value is consistently around 30 vol % H_2O. To obtain a more quantitative measure, we fitted a straight line to the data (Figure 2b), excluding the deviation at high contrast (see discussion on multiple scattering that follows below). Match points, $\sqrt{I} = 0$, were obtained at 30.4 ± 1.2 vol % H_2O and 31.6 ± 0.3 vol % H_2O in D_2O. The estimated SLD of the particles is 4.28 ± 0.18 × 10^{-6} $Å^{-2}$ and 4.20 ± 0.18 × 10^{-6} $Å^{-2}$, respectively. This is in good agreement with the expected match point of silica (literature value of SLD 4.1 × 10^{-6} $Å^{-2}$), corresponding to 32.4 vol % H_2O. The same is true for a system with 10 vol % solid content, as shown in Figure 3b, where the match point was determined with the estimated SLD of 4.28 ± 0.06 × 10^{-6} $Å^{-2}$ or 4.26 ± 0.07 × 10^{-6} $Å^{-2}$. The results also confirmed that up to 10 vol % SiO_2 there was no solid concentration dependency on the match point.

Ideally, there should be a linear relationship between $\sqrt{I}$ and H_2O vol % for a binary contrast system, q-dependent deviations from this indicate multiple scattering effects. These effects are anticipated to increase with H_2O vol % (i.e., contrast between solvent and particles) and be more

pronounced at low q than at high q. This effect is illustrated in Figures 2b and 3b: at the higher q-values (q_2 and q_3) there is a clear linear relationship. For the lower q-values (q_1), the $\sqrt{I}$ curves flatten as they become increasingly affected by multiple scattering. At 5 vol % silica sample, multiple scattering is visible for q_1 at the highest contrast of 70 vol % H_2O (Figure 2b), and for the 10% sample this is already visible for q_1 at 60 vol % H_2O (Figure 3b). Scattering data normalized to the intensity at about q_2, a q-region that does not appear to be affected by multiple scattering, are shown in Figures 2c and 3c. It can be seen that for 5 vol % silica sample (Figure 2c), the curves after normalization are very similar, and thus multiple scattering effects are not obvious. The curve at 40/60 appears to be slightly higher in intensity at low q, and we attribute this to small variations in sample preparation. For 10 vol % silica sample, however, the low q part shows a clear dependency on the contrast. Clearly the sample at the highest contrast (70 vol % H_2O) has lower intensity at low q than those with less contrast (Figure 2c), which is a typical sign of multiple scattering. Please also note that the samples at 30/70, which are very close to the match point, appear to be slightly lower at low q. Since this cannot be a sign of multiple scattering, we suggest that this can be attributed to heterogeneities in the SLD of the particles, possibly due to density variations around their average value, which can cause an effect that is only visible very close to the match point.

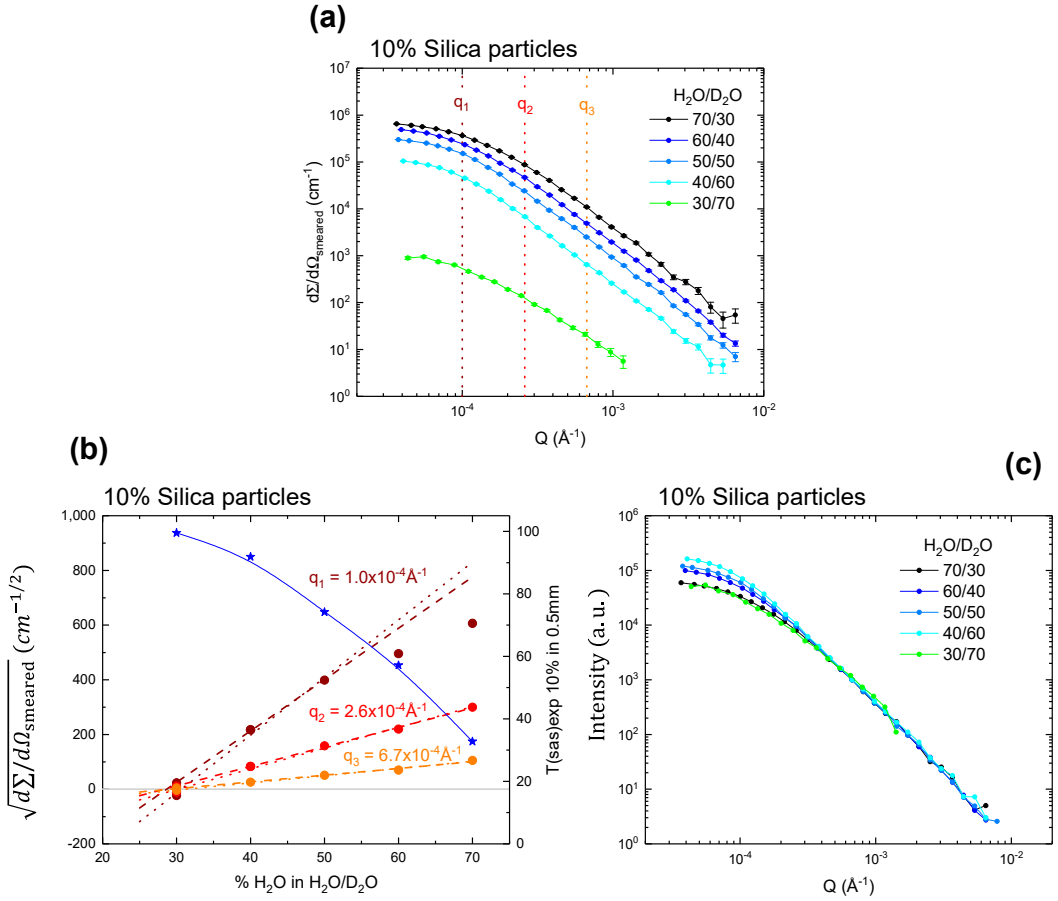

Figure 3. Contrast variation with 10 vol % SiO_2 at pH 10. (**a**) Scattering curves of samples with different H_2O/D_2O ratios; (**b**) left axis: the square root of the scattering intensity as a function of vol % H_2O in H_2O/D_2O ratio and q value (brown, red, and orange symbols for the three distinct q-values). The fitted line corresponds to the data with a positive sign (dashed line) and negative sign (dotted line) sign for the first point, respectively. Right axis: $T_{SAS,exp}$ in 0.5 mm path length (blue stars) as a function of vol % H_2O in H_2O/D_2O ratio; (**c**) a plot of the scattering curves from (**a**) normalized to the same value at high q.

Another measure that can be used as a guide to evaluate the probability of multiple scattering, is the so-called T_{SAS} value. This corresponds to the fraction of the beam that passes through the sample without being scattered [38,39]. The T_{SAS} value of a sample is experimentally determined as the ratio between the transmission of the direct beam (T_{Rock}, as measured on the main detector) and the overall transmission of the direct beam and scattering pattern (T_{Wide}, as measured on the transmission detector) and it can also be theoretically estimated. The definitions of these three values are given in the Equations (5)–(7). Equation (8) was used for the theoretical estimation where Φ is the volume fraction of particles, (Δ_{SLD}) is the neutron contrast between the particles, $SLD_{particle}$, and the liquid, $SLD_{solvent}$, whose definition is given in the Equations (9) and (10); D is the diameter of the particle, L is the sample thickness, Φ_{H_2O} is the volume fraction of H_2O, and Φ_{D_2O} is the volume fraction of D_2O. As a guide, the ideal value for T_{SAS} is above 0.9 (90%) [39]. A T_{SAS} value well above 0.9 indicates that the scattering signal is rather weak for USANS with a reduced probability of multiple scattering, while a decrease in a T_{SAS} value below 0.9 indicates that there is an increased probability of multiple scattering. The T_{SAS} value can be a very useful tool as a guide to the expected degree of multiple scattering [38–40]. Note however, that the effect of multiple scattering on scattering curves is q-dependent (see discussion below), and a higher degree of multiple scattering can be tolerated if the scattering curves do not show sharp features even in the single scattering regime.

In this study, we also used T_{SAS} values to discuss the effect of multiple scattering in two different geometries (i.e., flat cell, flow cell), and consequentially different path-lengths, under different solid concentrations, and H_2O/D_2O ratios, coupling with changes in the scattering intensity.

$$T_{SAS,\mathrm{exp}} = \frac{T_{rock}}{T_{wide}} \tag{5}$$

$$T_{Rock} = \frac{I_{sample(direct\ beam)}}{I_{empty\ cell(direct\ beam)}} \tag{6}$$

$$T_{Wide} = \frac{I_{sample(direct\ beam\ plus\ scattering\ pattern)}}{I_{empty\ cell(direct\ beam\ plus\ scattering\ pattern)}} \tag{7}$$

$$T_{SAS,\mathrm{est}} = e^{-(\frac{3}{4}\lambda^2\Phi(1-\Phi)(\Delta_{SLD})^2DL)} \tag{8}$$

$$\Delta_{SLD} = SLD_{particle} - SLD_{solvent} \tag{9}$$

$$SLD_{solvent} = \Phi_{H_2O}SLD_{H_2O} + \Phi_{D_2O}SLD_{D_2O} \tag{10}$$

Table 1 shows the T_{SAS} values with different H_2O/D_2O ratios for a system with 5 and 10 vol % solid content in the tumbling cell with a thickness of 0.5 mm. Table 1 also shows the theoretically estimated T_{SAS} values for the same samples, based on Equation (8). The parameter in this Equation that is not precisely known is the effective particle size D (it is a polydisperse system). This value was manually adjusted to 2.25 µm to give very good agreement for the T_{SAS} values at all investigated contrasts for both the 5 vol % and 10 vol % silica sample. This value was also in good agreement with the average particle size obtained for this sample from laser diffraction (2.4 µm). This good agreement gave us confidence to use this formula to estimate the optimal H_2O/D_2O ratio for the Couette cell (thickness = 1 mm) for rheo-SANS (see Table 1). The nominal/path-length thickness of the flow cell is close to 1 mm, double of the tumbling cell thickness (0.5 mm).

Table 1. Scattering length density (SLD) and T_{SAS} values experimentally determined ($T_{SAS,exp}$) at 5 vol % SiO_2 and 10 vol % SiO_2 at pH 10 with 0.5 mm path length, respectively. Also shown are the corresponding calculated values $T_{SAS,\ est}$ for the thickness of 0.5 mm and 1 mm, using Equation (8) *.

vol.% H_2O/D_2O	**$SLD_{(ave)}$, $Å^{-2}$**	**Flat cell**						**Flow cell**	
		$T_{sas,\ exp}$		**$T_{sas,est}$**				**$T_{sas,\ exp}$**	
		5 vol.% SiO_2 in 0.5 mm	10 vol.% SiO_2 in 0.5 mm	5 vol.% SiO_2 in 0.5 mm	10 vol.% SiO_2 in 0.5 mm	5 vol.% SiO_2 in 1 mm	10 vol.% SiO_2 in 1 mm	5 vol.% SiO_2	10 vol.% SiO_2
30/70	4.31×10^{-6}	101%	100%	100%	99%	99%	99%		
40/60	3.62×10^{-6}	98%	92%	98%	96%	96%	92%	100%	92%
50/50	2.94×10^{-6}	83%	74%	88%	79%	78%	63%		
60/40	2.25×10^{-6}	64%	57%	73%	56%	54%	31%		
70/30	1.56×10^{-6}	51%	33%	56%	33%	31%	11%		

* The calculations are based on the literature value for the SLD of silica particles, and the particle size was used as an adjustable parameter to get good agreement between the experimental and calculated values. It was fixed to 2.25 μm (close to the experimentally measured value of 2.4 μm by laser diffraction). The error in experimental T_{SAS} values is estimated to be about 4%.

The experimentally determined T_{sas} values were also plotted in Figures 2b and 3b (blue stars) in order to investigate their correlation with the scattering intensity as a function of vol % H_2O in H_2O/D_2O. It can be noticed that for the 5 vol % silica particle suspensions T_{sas} values above 60% maintained good linearity on the square scattering intensity until 60 vol % H_2O in H_2O/D_2O ratio at the lowest q range plotted (1×10^{-4} A^{-1}), showing only a negligible effect of multiple scattering (Figure 2b). At 10 vol % silica particle suspensions, above 70% T_{sas} value maintained the linearity, up to 50 vol % H_2O/D_2O ratio (Figure 3b). On the other hand, for the higher q ranges (2.6×10^{-4} A^{-1}, 6.7×10^{-4} A^{-1}), there was no deviation from the linearity for the both 5 and 10 vol % silica particle suspension, indicating that the effect of multiple scattering present in those systems is minimal (if not absent) with these q ranges.

Based on these results, 40 vol % H_2O was selected for the rheo-setup to reduce multiple scattering ($T_{SAS,est}$ = 96% and 92.5% at 1 mm path length for the 5 vol % and 10 vol % sample, see Table 1) while optimizing the scattered intensity. Figure 4 shows the scattering curve comparison between the measurements using a flat cell with tumbling motion and the Couette geometry for rheo-USANS at a shear rate of 500 s^{-1}. This shear rate was selected as it is well above the minimum rate that ensured good particle dispersion during the measurement for comparison with the tumbling flat cell. The viscosity of the suspension was measured at increasing constant shear rates for a fixed period of time (peak hold test). The minimum shear rate to maintain a constant viscosity was determined and higher shear rate than the minimum was tested (500 s^{-1}).

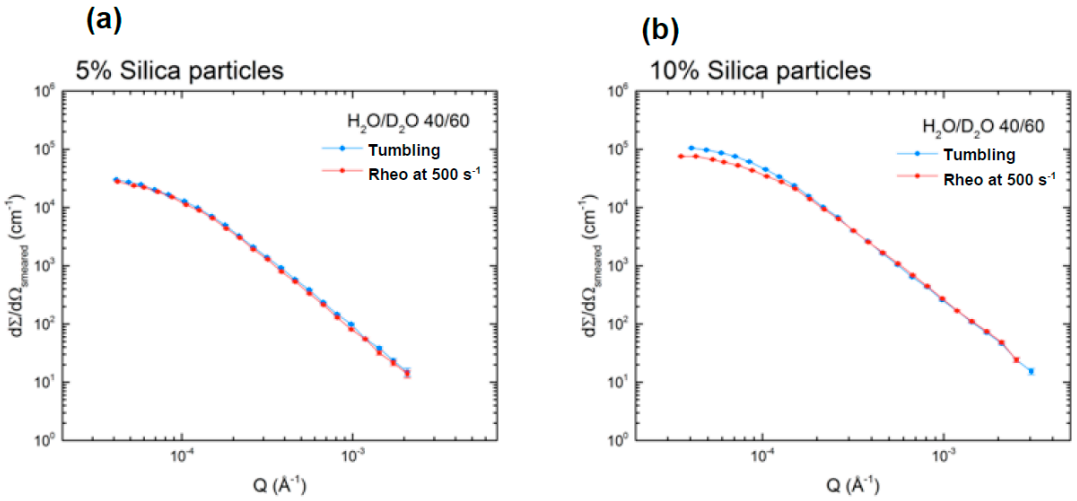

Figure 4. Scattering curve comparison between measurements using a flat cell with tumbling motion and Couette geometry for rheo-USANS at 500 s^{-1} shear rate. (**a**) 5 vol % SiO_2, 40 vol % H_2O in H_2O/D_2O ratio, pH10; (**b**) 10 vol % SiO_2, 40 vol % H_2O in H_2O/D_2O ratio, pH10.

It can be seen that there is a very good agreement, for the 5 vol % silica sample (Figure 4a), between the shape of the scattering curves of the sample in the tumbling cell and in the rheo-cell at 500 s^{-1}, measured independently. The thickness of the rheo-cell during data reduction, which impacts on the overall intensity scale, was chosen to be 1 mm and the good agreement in the intensity to the data in tumbling mode imply that the curvature of the rheo-cell was not significant to increase the value of the effective sample thickness significantly. At 10 vol % (Figure 4b), we observed that the scattering curves slightly deviate at low q between these two scenarios. The experimental T_{SAS} values for the 5 vol % and 10 vol % silica sample, Table 1, clearly show that both these samples should not be in a range, where multiple scattering is pronounced. We therefore conclude that this difference for the 10 vol % sample is a real structural change that is caused by the Couette shear. We suggest that Couette shear gives a better particle dispersion than simple tumbling motion. In other words, there were less aggregates present in the rheometer.

Table 2 shows the T_{SAS} values determined at different experimental conditions, such as solid/particle concentration, pH, and shear rate. Regardless of the experimental conditions varied, T_{SAS} values were generally high enough (>90%) to reduce multiple scattering effects. For higher silica concentration at 20 and 40 vol %, we anticipated even more multiple scattering than 5 and 10 vol % (if we do not apply contrast variation). Thus, we selected slightly less H_2O vol %—i.e., 37—compared with the value suggested (40 vol % H_2O) for less silica vol %. This yielded high T_{SAS} values in general, i.e., minimization of effects of multiple scattering.

There is a slight decrease in T_{sas} values with increasing the shear rate. It indicates the presence of slightly more scattering that can be explained by the structural effects due to shear thickening behavior of concentrated silica suspensions forming particle clustering [30]. Small degree of thickening (i.e., small increase in viscosity) observed during the shear tests can explain the small change in T_{sas} value. Thus, samples showing significant thickening behavior could largely reduce the T_{sas} value that should be experimentally evaluated. Studying the effects of changes in particle/aggregate structure on multiple scattering effects with the application of contrast variation can be a good future study topic in this field.

Anovitz and Cole 2015 [11] reported that the thickness required for minimizing multiple scattering effects and having T_{SAS} value of higher than 90% is approximately below 0.15 mm without contrast variation. In comparison, our sample thicknesses were 0.5 mm in a flat cell and 1 mm in a rheo-cell that is up to the factor of 7 and still achieved minimizing multiple scattering effects, shown by T_{SAS} values higher than 90%.

Table 2. T_{SAS} values experimentally determined from rheo-USANS measurements. The error in experimental T_{SAS} values is estimated to be about 4%.

SiO_2 vol.%	H_2O%	pH	Shear rate (s^{-1})	$T_{(SAS)exp}$
5	40	10	250 500 1000	102% 101% 102%
10	40	10	250 500 1000	94% 92% 90%
5	40	2	500 1000	98% 99%
10	40	2	500 1000	96% 97%
20	37	10	500 1000 2000	98% 97% 94%
20	37	2	500 1000 2000	96% 92% 91%
40	37	2	5 50 500 1000	94% 95% 95% 77%
40	37	10	50 500 1000 2000	99% 99% 100% 99%

4. Conclusions

The effect of H_2O/D_2O ratio was studied in terms of the scattering intensity and transmission at different q values in order to further understand and reduce multiple scattering effects that can be present in concentrated colloidal particle suspensions and maintain strong enough scattering signals. We used two different sample geometries (i.e., flat cell, rheo-cell) with different silica vol %, and identified the changes in the square of scattering intensity ($\sqrt{I}$) and transmission of silica particle suspensions. In general, the deviations of the linearity of $\sqrt{I}$, i.e., indication of multiple scattering only observed at low q, well correlated with the decrease in the transmission that were evaluated by T_{SAS} values. The comparison between the experimentally determined and theoretically calculated T_{SAS} values showed good agreement. Thus, theoretical calculations were also applied to estimate the T_{SAS} values in different sample thickness and the selection of H_2O/D_2O ratio for rheo-USANS experiments. It was found that H_2O/D_2O contrast variation is a good method to achieve the objectives of reducing multiple scattering effects of colloidal particle suspensions for both ultra-small-angle neutron scattering (USANS) and rheo-USANS experiments even for highly concentrated silica suspensions up to 40 vol %.

Author Contributions: Conceptualization, A.O. and C.J.G.; Formal analysis, A.O. and L.d.C.; Funding acquisition, A.O.; Investigation, A.O. and L.d.C.; Methodology, A.O., L.d.C., C.J.G. and C.R.; Project administration, A.O.; Resources, A.O.; Supervision, A.O.; Validation, A.O., L.d.C., C.J.G. and C.R.; Visualization, A.O. and L.d.C.; Writing—original draft, A.O.; Writing–review & editing, A.O., L.d.C., C.J.G. and C.R.

Funding: Akira Otsuki would like to acknowledge the support for his travel to perform neutron scattering experiments at ANSTO from the scientific mobility program between France and Australia as well as the Observatoire Terre Environnement Lorraine (OTELo).

Acknowledgments: We acknowledge support of the Australian Centre for Neutron Scattering (ACNS) at the Australian Nuclear Science and Technology Organisation (ANSTO), in providing the neutron research facilities used in this work.

Conflicts of Interest: The authors declare no conflict of interest.

References

1. Crawford, R.; Ralston, J. The influence of particle size and contact angle in mineral flotation. *Int. J. Miner. Process.* **1988**, *23*, 1–24. [CrossRef]
2. Otsuki, A.; Bryant, G. Characterization of the interactions within fine particle mixtures in highly concentrated suspensions for advanced particle processing. *Adv. Colloid Interface Sci.* **2015**, *226*, 37–43. [CrossRef] [PubMed]
3. Otsuki, A. Coupling colloidal forces with yield stress of charged inorganic particle suspension: A review. *Electrophoresis* **2018**, *39*, 690–701. [CrossRef] [PubMed]
4. Kralchevsky, P.A.; Danov, K.D.; Denkov, N.D. Chemical physics of colloid systems and interfaces. In *Handbook of Surface and Colloid Chemistry*, 3rd ed.; Birdi, K.S., Ed.; CRC Press: Boca Raton, FL, USA, 2008; Chapter 7, pp. 197–377.
5. Stepanek, P. Static and dynamic properties of multiple light scattering. *J. Chem. Phys.* **1993**, *99*, 6384–6393. [CrossRef]
6. Boger, D.V. Rheology and the resource industries. *Chem. Eng. Sci.* **2009**, *64*, 4525–4536. [CrossRef]
7. Franks, G.V. Innovative applications of controlled particle interactions. *Chem. Eng. Res. Des.* **2005**, *83*, 937–946. [CrossRef]
8. Kalman, D.P.; Wagner, N.J. Microstructure of shear-thickening concentrated suspensions determined by flow-USANS. *Rheol. Acta* **2009**, *48*, 897–908. [CrossRef]
9. Feigin, L.A.; Svergun, D.I.; Taylor, G.W. General principles of small-angle diffraction. In *Structure Analysis by Small-Angle X-ray and Neutron Scattering*; Springer: Boston, MA, USA, 1987; pp. 25–55.
10. Šaroun, J. Evaluation of double-crystal SANS data influenced by multiple scattering. *J. Appl. Cryst.* **2000**, *33*, 824–828. [CrossRef]
11. Anovitz, L.M.; Cole, D.R. Characterization and analysis of porosity and pore structures. *Rev. Mineral. Geochem.* **2015**, *80*, 61–164. [CrossRef]
12. Debye, P.; Bueche, A.M. Scattering by an inhomogeneous solid. *J. Appl. Phys.* **1949**, *20*, 518–525. [CrossRef]
13. Cousin, F. Small angle neutron scattering. *EPJ Web Conf.* **2015**, *104*. [CrossRef]

14. NIST Center for Neutron Research. Neutron Activation Calculator. 2016. Available online: https://www.ncnr.nist.gov/resources/activation/ (accessed on 10 July 2017).
15. Vineyard, G.H. Multiple scattering of neutrons. *Phys. Rev.* **1954**, *96*, 93–98. [CrossRef]
16. Blech, I.A.; Averbach, B.L. Multiple scattering of neutrons in vanadium and copper. *Phys. Rev.* **1965**, *137*, 1113. [CrossRef]
17. Sears, V.F. Slow-neutron multiple scattering. *Adv. Phys.* **1975**, *24*, 1–45. [CrossRef]
18. Schelten, J.; Schmatz, W. Multiple-scattering treatment for small-angle scattering problems. *J. Appl. Cryst.* **1980**, *13*, 385–390. [CrossRef]
19. Soper, A.K.; Egelstaff, P.A. Multiple scattering and attenuation of neutrons in concentric cylinders: I. Isotropic first scattering. *Nucl. Instrum. Meth.* **1980**, *178*, 415–425. [CrossRef]
20. Goyal, P.S.; King, J.S.; Summerfield, G.C. Multiple scattering in small-angle neutron scattering measurements on polymers. *Polymer* **1983**, *24*, 131–134. [CrossRef]
21. Berk, N.F.; Hardman-Rhyne, K.A. Analysis of SAS data dominated by multiple scattering. *J. Appl. Cryst.* **1988**, *21*, 645–651. [CrossRef]
22. Andreani, C.; Merlo, V.; Ricci, M.A. A procedure for multiple scattering corrections in a neutron incoherent inelastic scattering experiment. *Nucl. Instrum. Methods Phys. Res. Sect. B Beam Interact. Mater. At.* **1989**, *36*, 216–221. [CrossRef]
23. Mazumder, S.; Bhagwat, K.V.; Sequeira, A. Estimation of particle size distribution in multiple small-angle scattering. *J. Phys. Condens. Matter* **2003**, *7*, 9737–9746. [CrossRef]
24. Copley, J.R.D. The significance of multiple scattering in the interpretation of small-angle neutron scattering experiments. *J. Appl. Cryst.* **1988**, *21*, 639–644. [CrossRef]
25. Davidowski, J.; Granada, J.R.; Mayer, R.E.; Cuello, G.J.; Gillette, V.H.; Bellissent-Funel, M.C. Multiple scattering and inelasticity corrections in thermal neutron scattering experiments on molecular systems. *Phys. B Condens. Matter* **1994**, *203*, 116–128. [CrossRef]
26. Rodríguez Palomino, L.A.; Dawidowski, J.; Blostein, J.J.; Cuello, G.J. Data processing method for neutron diffraction experiments. *Nucl. Instrum. Methods Phys. Res. Sect. B Beam Interact. Mater. At.* **2007**, *258*, 453–470. [CrossRef]
27. Mancinelli, R. Multiple neutron scattering corrections. Some general equations to do fast evaluations. *J. Phys. Conf. Ser.* **2012**, *340*, 012033. [CrossRef]
28. Sabine, T.M.; Bertram, W.K. The use of multiple-scattering data to enhance small-angle neutron scattering experiment. *Acta Cryst. A Found. Crystallogr.* **1999**, *55*, 500–507. [CrossRef]
29. Connolly, J.; Bertram, W.; Barker, J.; Buckley, C.; Edwards, T.; Knott, R. Comparison of the structure on the nanoscale of natural oil-bearing and synthetic rock. *J. Petrol. Sci. Eng.* **2006**, *53*, 171–178. [CrossRef]
30. Mewis, J.; Wagner, N.J. *Colloidal Suspension Rheology*; Cambridge University Press: New York, NY, USA, 2012; Chapters 8 and 9, pp. 252–324.
31. Rehm, C.; Brûlé, A.; Freund, A.K.; Kennedy, S.J. Kookaburra: The ultra-small-angle neutron scattering instrument at OPA. *J. Appl. Crystallogr.* **2013**, *46*, 1699–1704. [CrossRef]
32. Rehm, C.; de Campo, L.; Brûlé, A.; Darmann, F.; Bartsch, F.; Berry, A. Design and performance of the variable-wavelength Bonse–Hart ultra-small-angle neutron scattering diffractometer KOOKABURRA at ANSTO. *J. Appl. Crystallogr.* **2018**, *51*, 1–8. [CrossRef]
33. Bonse, U.; Hart, M. Tailless X-ray single-crystal reflection curves obtained by multiple reflection. *Appl. Phys. Lett.* **1965**, *7*, 238–240. [CrossRef]
34. Kline, S.R. Reduction and analysis of SANS and USANS data using IGOR Pro. *J. Appl. Crystallogr.* **2006**, *39*, 895–900. [CrossRef]
35. Xiong, N.; Mannicke, D.; Lam, T.; Hauser, N. *Gumtree Application for Neutron Scattering*, version 1.13; Zenodo: Geneve, Switzerland, 2017. [CrossRef]
36. Kent, B.; Hunt, T.; Darwish, T.A.; Hauss, T.; Garvey, C.J.; Bryant, G. Localization of trehalose in partially hydrated DOPC bilayers: insights into cryoprotective mechanisms. *J. R. Soc. Interface* **2014**, *11*, 20140069. [CrossRef] [PubMed]
37. Furlong, E.J.; Choudhury, H.G.; Kurth, F.; Duff, A.P.; Whitten, A.E.; Martin, J.L. Disulfide isomerase activity of the dynamic, trimeric Proteus mirabilis ScsC protein is primed by the tandem immunoglobulin-fold domain of ScsB. *J. Bio. Chem.* **2018**, *293*, 5793–5805. [CrossRef] [PubMed]

38. Rehm, C.; Barker, J.; Bouwman, W.G.; Pynn, R. DCD USANS and SESANS: a comparison of two neutron scattering techniques applicable for the study of large-scale structures. *J. Appl. Crystallogr.* **2013**, *46*, 354–364. [CrossRef]
39. Jackson, A.; Kline, S.; Barker, J.; Mildner, D. *SANS and USANS Investigation of Oil Uptake by Micellar Gels*; Tutorial on Ultra Small Angle Neutron Scattering; NIST Center for Neutron Research: Gaithersburg, MD, USA, 2008.
40. *Characterization of Latex Microspheres with USANS*; NIST Center for Neutron Research: Gaithersburg, MD, USA, 2004.